

Identification of residual nano-scale foulant material on stainless steel using atomic force microscopy after clean in place

Phinney, David; Goode, Kylee; Fryer, Peter; Heldman, Dennis; Bakalis, Serafeim

DOI:

[10.1016/j.jfoodeng.2017.06.019](https://doi.org/10.1016/j.jfoodeng.2017.06.019)

License:

Creative Commons: Attribution-NonCommercial-NoDerivs (CC BY-NC-ND)

Document Version

Peer reviewed version

Citation for published version (Harvard):

Phinney, D, Goode, K, Fryer, P, Heldman, D & Bakalis, S 2017, 'Identification of residual nano-scale foulant material on stainless steel using atomic force microscopy after clean in place', *Journal of Food Engineering*. <https://doi.org/10.1016/j.jfoodeng.2017.06.019>

[Link to publication on Research at Birmingham portal](#)

General rights

Unless a licence is specified above, all rights (including copyright and moral rights) in this document are retained by the authors and/or the copyright holders. The express permission of the copyright holder must be obtained for any use of this material other than for purposes permitted by law.

- Users may freely distribute the URL that is used to identify this publication.
- Users may download and/or print one copy of the publication from the University of Birmingham research portal for the purpose of private study or non-commercial research.
- User may use extracts from the document in line with the concept of 'fair dealing' under the Copyright, Designs and Patents Act 1988 (?)
- Users may not further distribute the material nor use it for the purposes of commercial gain.

Where a licence is displayed above, please note the terms and conditions of the licence govern your use of this document.

When citing, please reference the published version.

Take down policy

While the University of Birmingham exercises care and attention in making items available there are rare occasions when an item has been uploaded in error or has been deemed to be commercially or otherwise sensitive.

If you believe that this is the case for this document, please contact UBIRA@lists.bham.ac.uk providing details and we will remove access to the work immediately and investigate.

Accepted Manuscript

Identification of residual nano-scale foulant material on stainless steel using atomic force microscopy after clean in place

David M. Phinney, Kylee Goode, Peter J. Fryer, Dennis Heldman, Serafim Bakalis



PII: S0260-8774(17)30265-0

DOI: [10.1016/j.jfoodeng.2017.06.019](https://doi.org/10.1016/j.jfoodeng.2017.06.019)

Reference: JFOE 8924

To appear in: *Journal of Food Engineering*

Please cite this article as: David M. Phinney, Kylee Goode, Peter J. Fryer, Dennis Heldman, Serafim Bakalis, Identification of residual nano-scale foulant material on stainless steel using atomic force microscopy after clean in place, *Journal of Food Engineering* (2017), doi: 10.1016/j.jfoodeng.2017.06.019

This is a PDF file of an unedited manuscript that has been accepted for publication. As a service to our customers we are providing this early version of the manuscript. The manuscript will undergo copyediting, typesetting, and review of the resulting proof before it is published in its final form. Please note that during the production process errors may be discovered which could affect the content, and all legal disclaimers that apply to the journal pertain.

1 **Title**

2 Identification of residual nano-scale foulant material on stainless steel using atomic force microscopy
3 after clean in place

4

5 **Authors**

6 David M. Phinney^{a,b}, Phinney.14@osu.edu (Corresponding author)

7 Kylee Goode^b, k.r.goode@bham.ac.uk

8 Peter J Fryer^b, p.j.fryer@bham.ac.uk

9 Dennis Heldman^{a,c}, heldman.20@osu.edu

10 Serafim Bakalis^b, s.bakalis@bham.ac.uk

11 ^aThe Ohio State University, Department of Food Science & Technology.

12 2015 Fyffe Ct., Columbus OH 43210. USA

13 ^bUniversity of Birmingham, School of Chemical Engineering

14 Edgbaston, Birmingham, West Midlands, B15 2TT. UK

15 ^cThe Ohio State University, Department of Food, Agriculture and Environmental Science

16 590 Woody Hayes Drive, Columbus, OH 43210. USA

17

18

19 **Abstract**

20 During clean-in-place (CIP), solutions are pumped through process equipment to remove soils having
21 adverse effects on production. In order to validate reductions in CIP inputs, foulants need to be
22 detectable and quantifiable on smaller scales than current industrial practices. In this study, fluorescent
23 microscopy was used for quantifying macroscopic cleanliness of a soiled stainless steel coupon after CIP.
24 An asymptotic model was used to describe the removal of soil as a function of the coupon exposure
25 time and cleaning solution temperature. From these models, cleaning parameters were determined and
26 used to generate coupons predicted to be 99.0 and 99.9% clean. This cleanliness was verified using
27 atomic force microscopy (AFM). AFM identified foulant on the order of $5 \mu\text{m}^2$ on a $1.0 \times 10^4 \mu\text{m}^2$ area.
28 AFM showed cleanliness ranging from 99.41 to 99.94 %. Differences between predicted and actual
29 cleanliness suggest a change in cleaning mechanism at different scales.

30

31

32

33

34

35

36

37 **Key words**

38 Clean in place; atomic force microscopy; fluorescence microscopy; protein fouling; thermal processing

39 1. Introduction

40 The process of cleaning in place (CIP) is typically achieved by pumping large volumes of cleaning
41 solution (most commonly detergents or strong bases) through process pipelines and sprayed on tank
42 walls to remove residual deposits from contact surfaces (Heldman and Lund, 2007). There are variations
43 on CIP steps but all of them would contain a “cleaning” step. During the cleaning step (which usually
44 comes after a pre-rinse of the system with water) detergent solutions are pumped through the system
45 to remove strongly adhered deposits. Several CIP variables surrounding the detergent solutions have
46 been investigated in the past for their significance in effective cleaning during CIP (Fickak et al., 2011;
47 Gillham et al., 1999; Jeurnink and Brinkman, 1994). Recently, the area of CIP has developed interest
48 from industrial perspectives because reduction in water inputs to cleaning operations can reduce total
49 plant water consumption significantly (Tiwari et al., 2016). To this effect, researchers have specifically
50 begun to investigate reductions in water, chemical, electrical energy and time consumption during CIP.
51 Reductions in total inputs to a CIP operation must maintain hygiene after a CIP operation is complete.
52 Furthermore, despite various advances in CIP research and technology, industries often use a visual
53 check to validate CIP protocols (Forsyth et al., 2006). Therefore, advances in defining a clean contact
54 surface on smaller scales must be developed in an effort to better quantify the effect of reducing CIP
55 inputs (water, chemicals and energy). Without better defining “how clean is clean,” clean process
56 technology advances are limited (Bakeev, 2010; Jones et al., 2012).

57 In cleaning research, the size of deposit is an important variable to define, especially when
58 comparing deposits of different magnitudes. ‘Length’ scales to describe the size of deposits in cleaning
59 and fouling research have been previously presented (Akhtar et al., 2010). The presented scale describes
60 fouling layers ranging from millimeter lengths (e.g. residual thick material in tanks or lines after
61 processing) down to nanometer lengths (e.g. molecules on a contact surface). There is a large range of

62 foulant materials ranging between the molecular level (very small) and thick films (very large). Included
63 in this range is the “meso” scale sized foulant materials. The Meso scale, although not perfectly defined,
64 represents a large majority of the body of cleaning research. Examples of meso scale foulants in food
65 manufacturing include heat exchanger burn on and mineral build up. Recent research has correlated the
66 meso scale adherence of foulant at the nano scale. Akhtar et al., (2010) investigated the force required
67 to remove a foulant adhered to various substrates on the meso scale using micro-manipulation
68 techniques, and subsequently compared that to the nano scale force of adherence using atomic force
69 microscopy (AFM). The authors found that there are correlations between meso and nano force
70 requirements when correcting for surface area. Similarly, the research completed in this paper uses a
71 fluorescence microscopy technique to create predictive cleaning models on the meso scale and compare
72 those models to predicted cleanliness at the nano scale.

73 Two types of forces have been previously described during the process of cleaning (Liu et al.,
74 2006). *Cohesive* forces are those that bond the foulant to itself, where *adhesive* forces bond the foulant
75 to the surface. Many cases have shown the cleaning process begins as primarily cohesive removal and
76 ends being entirely adhesive (Midelet and Carpentier, 2004; Palabiyik et al., 2014). Conditions that
77 determine which set of forces control the process, and how this can be altered, are largely unknown.
78 Furthermore, these two phases of foulant removal (adhesive and cohesive cleaning) predominate
79 differently on different sizes of foulant. For example large deposits (cm length scale) will primarily
80 undergo cohesive removal initially where small deposits (nm length scale) require primarily adhesive
81 forces. In the nano length scale, during cleaning, the removal of deposits can be considered entirely
82 adhesive (Bobe et al., 2007; Okorn-schmidt et al., 2014). The research performed here focuses on the
83 application of instrumentation developed for nano technology to investigate what is happening on a
84 molecular level towards the completion of a cleaning process.

85 In cleaning research, the method for quantifying hygiene level is clearly defined and governed
86 by the scale at which the investigation is pertinent. (Cole et al., (2010) investigated removal of large
87 deposits by completely filling an industrial pipe section with toothpaste and applying water to remove
88 the toothpaste. This scale is on the order of grams of deposit per area, or meters when discussing the
89 length scale of foulant previously defined. In this case, Cole et al., (2010) used turbidity and electrical
90 conductivity of the solution leaving the pipe as indicators of the removal of toothpaste from the pipeline
91 during a rinse with pure water (i.e. no detergents or other cleaning agents) where the solution was
92 directly pumped to the drain. Determining cleaning time at this scale is governed by the detection limits
93 of the instrumentation used and the removal of nanometer length sized deposits may have been
94 undetectable by the instrument response (Klahre and Flemming, 2000; Van Asselt et al., 2002). The
95 research performed in this manner, i.e. research that primarily focuses on large visual deposits, can be
96 considered macro-foulant research.

97 Other research has evaluated extremely sensitive instrumentation for detecting deposit
98 formation and removal on the nano lengths scale. Chen et al., (2010) and Favrat et al., (2012) used a
99 quartz crystal microbalance (QCM) which allows for real time determination of nano-gram amounts of
100 deposit on various substrates determined by changes in vibrational properties of the substrate itself.
101 The QCM technology provides knowledge of deposition and removal of foulants at the molecular level
102 but is also limited in range, which does not allow it to form a commercially relevant thickness of foulant
103 on the substrate.

104 A large body of academic literature focuses on the meso length scale. For example, whey
105 protein gels have been used to study the mass transfer of detergent in to a model foulant (Fickak et al.,
106 2011; Mercadé-Prieto et al., 2008; Mercadé-Prieto and Chen, 2006) at mm to micron scale . The passage
107 of chemicals in to the foulant deposit is the first necessary step in removing deposits which remain after

108 a water rinse. This concept is transferrable to the deposit on the nano length scale, because nano-scale
109 deposits of dairy based foulants need chemical modification prior to removal. This chemical
110 modification is governed by the rate of diffusion of cleaning agent in to deposit and therefore
111 represents a mass transfer step prior to either dissolution of the foulant or physical removal (peeling) of
112 the deposit (Changani et al., 1997; Fryer et al., 2006).

113 Deposits in the hundreds of nano grams of foulant per square centimeter represent the micro
114 length scale as well as that which can be considered primarily adhesive removal. Fan et al., (2015)
115 studied the removal of a dairy type foulant from the surface of commercial pipelines. Residual deposit
116 levels, after a rinse cycle was complete, were determined by extracting foulant residues from the inner
117 pipe surface in to a solution and subsequently determining the protein content of that solution. Here,
118 alkaline solutions were used to dissolve the remaining dairy based deposit in to solution and said
119 solutions protein level was used as an indicator for residual deposit in the pipe section. Limitations with
120 the degree of detection in this method are directly tied to the volume of extraction fluid and extraction
121 process. For example, too little extraction fluid used runs the risk of not removing 100 % of the
122 remaining foulant while too much fluid dilutes the concentration of protein in the extraction and
123 renders it below the detection limit of the assay.

124 It was the goal of this research to develop an analytical methodology to investigate “visual
125 cleanliness” using fluorescent microscopy and subsequently compare cleaning rates to the level of
126 hygiene on a nano-level using atomic force microscopy (AFM). AFM has been used previously to
127 characterize adhesion forces (Fang et al., 2000; Handojo et al., 2009). The focus of the research
128 presented in this paper was the use nano instrumentation to detect nano level residual foulant material
129 on food contact surfaces, subsequently employing methods to quantify the nano-deposit using image
130 processing. Multiple approaches to the detection and quantification of nano deposits using atomic force

131 microscopy were explored. This work differs from the majority of industrial cleaning research by
132 identifying the deposit itself *in situ* opposed to looking at the indicators of foulant in a cleaning solution.

133 2. Materials and methods

134 2.1 Substrate characterization

135 Square 2.54 x 2.54 cm stainless steel (316L type) coupons were used as the model food contact
136 substrate in this study. Coupons were polished to a mirror finish using automotive grade sand papers
137 and polishing compound. Coupons were analyzed using atomic force microscopy (AFM) in tapping mode
138 to characterize surface properties prior to use in experimentation. A Nanowizard II AFM (JPK
139 Instruments AG, Berlin, Germany) was used for all AFM analyses performed. For initial roughness
140 determination it was imperative that the coupons surface be clean. Because “clean” is focal point of the
141 research, it is important to note – in detail – this method. To achieve “clean” coupons, coupons (after
142 polishing) were cleaned using 2.0 % (wt./wt.) NaOH and distilled water at 80 °C under agitation for 1
143 hour. Coupons were removed and rinsed with 1.0 % (vol./vol.) aqueous solutions of HCl. Coupons were
144 subsequently soaked in hexane for 5 minutes and then acetone for another 5 minutes. All solvents were
145 HPLC grade solvents purchased from Fisher Scientific LLC. After removal from acetone, samples were
146 allowed to air dry and were then analyzed using the AFM. A 100 x 100 μm area was scanned with a 512 x
147 512 resolution. Cross sectional analysis was completed using JPKSPM Image Software. Surface
148 roughness (R_a), root mean square roughness (R_q) and peak to valley roughness (R_t) was determined for
149 all coupons used in this study. Results for initial surface characteristics are: $R_a = 95 \text{ nm} (\pm 17 \text{ nm})$, $R_q =$
150 $131(\pm 26 \text{ nm})$ and $R_t = 744 (\pm 142 \text{ nm})$. After AFM analysis, the coupons showed sufficient similarity in
151 roughness to justify their use in the present study.

152 2.2 Foulant deposition

153 Whey protein concentrate (WPC) solutions were used as the model foulant to be adhered to the
154 stainless steel substrate. 10 % (wt./wt.) solutions of WPC (CARBALEC 35, Carbery, Ballineen, Co Cork,
155 Ireland) were created by blending WPC powder with distilled water at room temperature while being
156 stirred with a magnetic stir bar on a stir plate for an hour or until homogenous. Significant effort was
157 made to minimize aeration of the solution during the mixing/hydration stage to minimize foaming and
158 denaturation of the proteins in solution. 1 ml of the WPC solution was then pipetted on to the stainless
159 steel coupon and the coupon was then heated at 75 °C for 1 hour on a hot plate. This time and
160 temperature profile was used because it minimized bubble formation (because it was well below 100 °C)
161 and allowed gelation of the solution. The heating process induced gelation as well as dehydrated the
162 foulant on to the coupon surface. The coupons were then cooled to room temperature before exposure
163 to clean in place conditions.

164 Consistency of the initial foulant deposit was tested by checking the increase in coupon mass
165 after heating. Since 1 ml of 10 % (wt./wt.) solution was applied to each coupon, the increase in mass
166 should be around 0.1 g (solids in 1 ml). Results showed mass was increased 0.114 (± 0.012) g.

167 2.3 Cleaning procedure

168 0.5 % (wt./wt.) solutions of NaOH were used as the clean in place (CIP) solution during this
169 study. 1000 g of solution was added to a 2 L (D = 6.25 cm) beaker and was stirred using a 4.5 cm stir bar
170 at 300 rotations per minute (RPM). The clean in place (CIP) variable of interest in this study was the
171 temperature of the caustic solution. Temperature and RPM was monitored and controlled by using
172 Adwin Scientific IKA heated stir plate (Adwin Scientific Direct, Schaumburg, Illinois, USA). Coupons were
173 exposed to 40, 55 and 70 °C cleaning solutions for varying periods of time by suspending the coupon in
174 the CIP solution using an attached string for exposure and removal to the solution. The coupon was
175 lowered so that the center face of the coupon was 0.06 m below the surface of the cleaning solution

176 with the coupon's back against the beaker wall. The temperature range was selected to ensure
177 significant separation of cleaning rates between the treatments.

178 To evaluate the flow conditions of the benchtop vessel, two approaches were utilized. Firstly,
179 the impeller Reynolds number (N_{Re_i}) was used to calculate turbulence level at each temperature
180 condition. N_{Re_i} (Eq. 1) is calculated as;

$$181 \quad N_{Re_i} = \frac{\rho ND^2}{\mu} \quad (1)$$

182 Where ρ is the density of water at T, N is rotations per second of the stir bar, D is the diameter of the stir
183 bar and μ is the viscosity of water at T. Values for density and viscosity of water were obtained from the
184 National Institute of Standards and Technology (NIST) database. The turbulence value for a stirred vessel
185 begins at $N_{Re} = 10,000$ (Sinnott, 1999). The corresponding N_{Re} values for 40, 55 and 70 °C are 15,400,
186 19,800 and 24,500 respectively. All of which correspond to a turbulent flow condition which would be
187 targeted during CIP. Although the N_{Re_i} represents turbulence at the tip of the impeller, with all other
188 conditions held constant (vessel size, volume of solution and rotational speed) it can be used to
189 correlate the relative turbulence changes between conditions.

190 The second approach at characterizing the flow conditions in the benchtop vessel was to create
191 a computational fluid dynamics (CFD) model of the design and extract various flow parameters from the
192 simulation. COMSOL Multiphysics (Version 5.2a, Palo Alto, California, USA) was used to create the
193 physical design of the system in a digital space. For the CFD model, the turbulent $k-\varepsilon$ flow was used with
194 the rotating machinery physics module to simulate the beaker stir bar combination. Average shear rate
195 over the coupon surface was extracted using the $rmspf.sr$ expression. Shear rate over the coupon
196 surface for 40, 55 and 70 °C was determined to be 62.3, 74.5 and 85.7 s^{-1} respectively. The CFD model
197 was also used to calculate the average velocity (by integration of the velocity profile distribution) from

198 the surface of the coupon, to 0.5 cm away from the surface. The average velocity was determined for
199 40, 55 and 70 °C to be 16.9, 17.3 and 17.5 cms^{-1} respectively. The slight changes in average velocity are
200 due to the changes in viscosity at the various temperatures in the mixing tank model.

201 It is important to clarify that the purpose of the research was not specifically to characterize the
202 effects of temperature on cleaning, rather the development of cleaning models at each temperature to
203 extend to the AFM evaluations. Exposure times at each temperature were selected by first visually
204 determining the time of removal foulant deposit under each condition. That time of (complete visual)
205 removal was then divided evenly in to 6-7 time points between initial exposure and the endpoint. After
206 removal from the cleaning solution, coupons were rinsed with ~25 ml of distilled water and heated at 75
207 °C on a hot plate for 30 minutes to drive off excess moisture and secure residual foulant material to the
208 coupon. After the CIP procedure, coupons were analyzed using fluorescent and atomic force
209 microscopy.

210 2.4 Fluorescent microscopy

211 2.4.1 Instrumentation and image acquisition

212 The aim of this study was to characterize the removal of a foulant from a “visual” cleanliness
213 method. In order to complete such an investigation, analytical methods for determining visual
214 cleanliness had to be developed. Because dairy proteins naturally fluoresce, fluorescent microscopy was
215 used as a surrogate to create an analytical method for visual cleanliness. Fluorescent images were taken
216 using a Leica digital microscope with a fluorescent light generator and digital filterset to look for
217 fluorescent light in the 410-420 nm range (Moro et al., 2001). Images were acquired using a XIMEA
218 MR285-MU (Ximea Corp., Golden, CO 80401, USA) at 10 times magnification using μ Manager software
219 as the camera controlling software. At this magnification, approximately 90% of the 2.54 x 2.54 cm
220 coupon was imaged, creating a macroscopic image of the coupon is its entirety. Significant effort was

221 made to control all aspects of image acquisitions and microscope adjustments to ensure identical image
222 parameters for each acquisition. The 8-bit images were taken and subsequently analyzed using ImageJ
223 (Schneider et al., 2012).

224 2.4.2 Clean vs. dirty

225 Cleanliness was determined by using the intensity of pixels in the 8-bit color space (256 shades
226 of grey). The histogram of color scores for a dirty coupon was achieved by imaging 6 coupons which had
227 been fouled by the aforementioned foulant deposition process. The fluorescent images were acquired
228 after a period of 30 s of exposure to fluorescent light to allow for stabilization of the photo bleaching.
229 Dirty coupons were evaluated in an identical manner but the coupon was cleaned using the same
230 solvent cleaning process from the substrate characterization process. Typical distribution frequency of
231 pixels for each of these can be seen in Fig. 1.

232 Fig. 1 shows a clear separation between the clean and dirty coupons at an approximate color
233 value of 41 to 51. Distributions of “clean” and “soiled” coupons were produced from 6 replicates and the
234 grey value separating those distributions was determined (by evaluating the minimum of the sum of the
235 two normal distributions) to be 45. Therefore, any pixel with a color score of 45 or above was
236 considered to fluoresce bright enough that it would be considered “dirty” and any pixel with a score less
237 than 45 was considered to be “clean.” There is a limitation in using fluorescence in that the intensity of
238 whey proteins decays with time (photo bleaching). Classifying pixels as soiled vs. clean after fluorescent
239 stabilization overcomes this issue. After the initial exponential decay (30 s) in fluorescent intensity (due
240 to photo bleaching) residue proteins still have significant intensity to have them identify as being “dirty.”

241 This evaluation method created a binary response from individual pixels in each image.
242 Therefore, a complex image of various pixel intensities was converted in to only clean and dirty pixels.
243 ImageJ was used to analyze the image and the percent area clean was calculated using Eq. 2.

$$A\% \text{ clean} = \left(1 - \frac{n_{\geq 45}}{N}\right) \times 100\% \quad (2)$$

245 Where $A\%$ is the percentage of area that is clean, $n_{\geq 45}$ is the sum total of the number of pixels in the
246 image with a color score of 45 or above and N represents the total number of pixels in the image. A
247 pictographic representation of the conversion of images from original image to percent clean can be
248 seen in Fig. 2.

249 2.4.3 Mathematical modeling

250 Fluorescent microscopy results were used to develop predictive models for the removal of the
251 foulant from the stainless steel coupons. To model the removal, a sigmoidal function was selected as the
252 fundamental equation. This was chosen for the following reasons;

- 253 (i) The method of cleaning used is based on color intensity rather than the thickness of foulant
254 in that pixel. Therefore, the process was predicted to have a larger induction cleaning period
255 where the foulant would be swelling and dissolving in to the cleaning solution (Mercadé-
256 Prieto and Chen, 2006). During this swelling phase, this image analysis method would return
257 a 100 % “dirty” response, even if some amount of layer ‘thickness’ had been removed.
- 258 (ii) Secondly, if the swelling and dissolution of the foulant was evenly distributed over the
259 coupon surface, then once “clean” pixels were exposed they would increase in number at
260 some rate as a function of time.
- 261 (iii) Lastly, there would have to be an asymptotic decay towards 100% “clean” pixel, as that is
262 the only end point.

263 Therefore, the sigmoidal growth model first proposed by Gompertz (Gompertz, 1825) was used in this
264 study. This model has been used and modified extensively throughout academic research primarily in
265 microbiological studies (Belda-Galbis et al., 2014; Chatterjee et al., 2014; Hossain et al., 2016). Although

266 seldom used in swelling/dissolution research such as this, the model has been successful in fitting the
267 various stages of microbial growth. The model used in this study can create sigmoidal curves which are
268 symmetric around a central value using Eq. 3.

$$269 \quad y = y_{max} e^{-e^{-k(t-t_m)}} \quad (3)$$

270 Here y_{max} represents the maximum cleanliness value attainable by the model, t is the continuous
271 variable of time, k represents the rate at which the sigmoid approaches its upper and lower asymptote
272 and t_m represents the time value at which $\frac{y}{y_{max}}$ is equal to e^{-1} . In this case y_{max} is equal to 100 % because
273 that is the maximum level of cleanliness so it is removed from the model. Therefore there are only two
274 parameter estimates needed to predict these sigmoidal functions from the fluorescent data; k and t_m .

275 2.4.4 Experimental design & statistical analysis

276 The fluorescent microscopy investigation was completed using a completely randomized design
277 which included 3 temperatures and 6 levels of time for the 70 °C condition, 7 levels of time for the 55 °C
278 condition and 8 levels of time for the 40 °C condition. PROC NLIN in SAS 9.4 (SAS Institute, Cary, North
279 Carolina, USA) was used to estimate model parameters (k and t_m) for the sigmoidal modeling of each
280 temperature. The standard error of the parameter estimates were used as goodness of fit parameters.

281 2.5 Atomic force microscopy

282 2.5.1 Time point selection method

283 Cleaning rates based on the fluorescent microscopy results were used to determine the cleaning
284 time variables needed for the atomic force microscopy analysis portion of the research. Two predicted
285 cleaning times were calculated from Equation 1 for each of the three temperatures (40, 55 and 70 °C).
286 The two cleaning times were predicted by calculating the time at which the coupons would be predicted

287 to be 99.0 and 99.9 percent clean. This created 6 variables for the AFM analysis (3 temperatures at 2
288 predicted cleanliness levels). This method was selected to investigate if the visual cleaning rate could be
289 translated and continued in to the non-visual scale. If that case was true, then each of the AFM images
290 for each level of predicted cleanliness would appear insignificantly different, *and* the difference in
291 cleanliness within a temperature between 99.0 and 99.9% clean would be distinguishable.

292 Samples for AFM analysis were fouled and subsequently exposed to CIP conditions for the
293 predetermined times. Samples were then rinsed with distilled water and washed with room
294 temperature (~ 23 °C) 1 % HCl to simulate an acid rinse which comes after the mid rinse step during the
295 CIP operation. This HCl rinse is meant to remove any mineral based deposits which may originate from
296 the fouling method, ensuring that any residual deposits detected could be considered a primarily
297 proteinaceous based matrix. After the HCl rinse, coupons were again rinsed with ~ 25 ml of distilled
298 water and dried on a 75 °C hot plate for approximately 30 minutes.

299 2.5.2 Surface topography

300 Surface topography of samples was evaluated using AFM contact mode with a silicon nitride
301 AFM tip with 0.32 N/m force constant (Part # PN-TR-TL-Au-20 A, Nanoworld AG, Neuchâtel,
302 Switzerland). Tips were calibrated for spring constant and resonance frequency each session. 100 x 100
303 μm areas were scanned with a 512 x 512 resolution and a tip speed of approximately 100 $\mu\text{m}/\text{s}$. Images
304 were processed using JPKSPM Data Processing Software. Images were corrected to have fixed
305 height/color values for direct comparison of the images and for further image analysis.

306 2.5.3 Force mapping

307 Samples identified to have residual deposits from the surface topography were evaluated using
308 a force mapping approach. The goal of force mapping was to correlate non-uniformities in surface

309 topographies with non-uniformities in attraction and repulsion forces between the tip and the surface.
310 Confirmation of distinguishability between “clean” stainless steel and residual nano-deposits using force
311 mapping could verify the existence of residual deposits even when the topography failed to identify it.
312 For instance, if a small deposit was to reside between two peaks of the substrate, the region would
313 appear smooth and clean from a topography evaluation. But if the force of integration responded
314 differently to fouled regions, this method could identify the deposit in this scenario.

315 Force mapped samples were evaluated using the tipless version of the AFM tip used in the
316 surface topography evaluation. A 30 nm diameter stainless steel sphere (part # SSMS-7.8 27-31um
317 0.2g, Copheric LLC, Santa Barbara, CA, USA) was adhered to the cantilever using two part epoxy and the
318 AFM controls. Again, 100 x 100 μm areas were mapped using 512 x 512 resolutions similar to what was
319 used in the surface topography evaluation.

320 3 Results & discussion

321 3.1 Fluorescent microscopy

322 Visual cleanliness determined by fluorescent microscopy results are presented in Fig. 3. Overlaid
323 on the raw data are the Gompertz sigmoidal models. Parameter estimates and standard errors from
324 each of these models are presented in Table 1. We can see that as the temperature of the cleaning
325 solution increases that the k value increases while t_m decreases. It has been well studied that increased
326 temperatures increases the cleaning rate (Fan et al., 2015; Gillham et al., 1999). The goal of this research
327 was to develop a method using fluorescent microscopy as a surrogate for visual cleanliness, not
328 specifically to study the effect of temperature. Simeone et al., (2016) used fluorescence imaging and
329 ultrasonic evaluation during the removal of chocolate sauce from stainless steel. Here, fluorescent
330 intensity was well correlated with foulant thickness and a real time model for removal of the chocolate
331 sauce were identified. The analytical methods in this paper are different than Simeone et al., (2016)

332 because thickness of the deposit could not be correlated with fluorescent intensity due to photo
 333 bleaching of whey proteins. Therefore, this research used a binary clean/dirty approach for images of
 334 fouled surfaces.

335 **Table 1: Table of the parameter estimates needed to create the fitted sigmoidal models on the fluorescent data (solid lines**
 336 **on Figure 2). The plus/minus refers to the standard error on the parameter estimate generated from SAS 9.4 PROC NLIN.**

Temp (°C)	k (s ⁻¹)	t_m (s)
40	0.064 ±0.01	92.0 ±1.1
55	0.25 ±0.05	49.1 ±0.4
70	0.41 ±0.03	32.7 ±0.2

337

338 The Gompertz sigmoidal growth model tended to fit the data quite well across the whole set with an
 339 average percent standard error of 9.76 % and 1.7 % for k and t_m respectively. The more interesting area
 340 of the sigmoid occurs at or near the value of t_m , where the error between replicates can be quite large.
 341 For example, after a 90 s exposure time at 40 °C the coupon cleanliness ranged (in the statistical sense
 342 of ‘range’) from 25 to 49 % clean between the three replicates. This error would then decrease purely
 343 from the assumption about the model once the process heads towards 100% clean. This suggests that at
 344 the levels beyond the detectable range of the fluorescent microscope that the errors decrease. It is
 345 important to understand that in this particular sigmoid model, the larger statistical distribution of raw
 346 values (i.e. “percent clean”) is highest towards t_m because this is the exponential portion of the model.
 347 Therefore, small differences in experimental error (say one extra second of exposure time from
 348 experimental error) has a large effect on the response. This is handled by the use of statistics to predict
 349 t_m , and even though the deviation of raw values is large at this value of t_m , the standard error is quite
 350 small. Similar methodologies for data processing are found in logarithmic transformation to data that is
 351 not identically distributed within the variables.

352 The use of direct fluorescent microscopy (opposed to say ATP fluorescence) on a commercial
 353 active heating surface, which has been processing dairy based, products is largely unknown. Future
 354 investigations should focus on how a foulant formed under commercial processing conditions responds
 355 to fluorescent exposure and how to intensify and quantify this foulant.

356 3.2 Atomic force microscopy

357 3.2.1 Surface topography

358 Using the results from Table 1 in the fluorescent microscopy portion of the research, the
 359 exposure times needed to achieve 2 “levels of cleanliness” (99.0 and 99.9 %) for each temperature were
 360 calculated using Equation 2. Table 2 shows these exposure times for the 6 variables (3 temperature and
 361 2 levels of cleanliness) used for the surface topography and the force mapping completed using atomic
 362 force microscopy (AFM).

363 **Table 2: Calculated exposure times for generation of samples to be analyzed using AFM. Values were calculated using the**
 364 **parameter estimates in Table 2 and solving for time in Equation 2.**

Temperature (°C)	Predicted exposure time (s)	
	99.0 % clean	99.9 % clean
40	165	200
55	65	100
70	45	60

365

366 Single image results for the surface topographies of each of these samples are presented in Fig.
 367 4. Here we can see when compared to the clean stainless steel surface, many of the samples have
 368 localized peaks which are up to 350 nm in height. These localized collections of peaks represent residual
 369 nano-foulant material on the surface which is not detectable through fluorescent microscopy because of
 370 its detection threshold being larger than AFM. Some interesting trends in residual deposit can be seen in
 371 the surface topographies. If we look across the 90.0 % clean coupons, samples are almost

372 indistinguishable from one another. The foulant islands in each of these maps are very similar in shape,
373 size and quantity. It is important to reiterate that these samples were exposed to cleaning solution for
374 very different period of times. The 40, 55 and 70 °C samples were exposed to 165, 65 and 45 s
375 respectively (as noted in Table 3). The results suggest that at the 99.0 % cleanliness level predicted
376 through fluorescence microscopy the removal rate parameters (k and t_m) hold true.

377 In contrast, when the topographies across the 99.9 % cleanliness level are compared, results
378 appear different. Although each time point here was predicated to have the same cleanliness, the
379 residual deposits on the surface increase with a decrease in temperature. Specifically, when looking at
380 the difference in surface topography between 99.0 and 99.9% clean at the CIP temperature of 40 °C, no
381 distinguishable difference in surface topographies can be identified, despite the predicted difference.
382 This suggests an alternative cleaning mechanism at the nano level during cleaning and removal of tightly
383 adhered deposits. Future work in this area should focus in investigating how the model changes as a
384 function of the scale at which CIP is working on.

385 Quantification of nano-deposits at this level proves significantly difficult. The variation in surface
386 topography of the stainless steel itself proves challenging to subtract out from the topographic images.
387 A Matlab™ code (V.R2013a, Mathworks inc., Massachusetts, USA) was developed using image
388 processing tools to convert AFM images to quantifiable values. The image extracted from JPKSPM
389 software was first converted to a black and white image and then converted to a binary image using a
390 threshold of 0.9. The thresholding value here needed to be set large enough that the peaks of the
391 stainless steel surface itself are removed. The binary image was processed in to morphological
392 structures using Matlab 'Strel' function to identify 'disk' objects in the binary image. The 'disks' were
393 then identified as foulant and percent cleanliness of each sample in the 100 x 100 μm area using Eq. 1

394 was estimated. Fig. 5 shows all the steps in this image process to extract quantitative data from the AFM
 395 topographical results. Table 3 shows the average results ($n = 2$) of cleanliness values for each condition.

396

397 **Table 3: Results for the percent cleanliness of the AFM samples analyzed by surface topography. Plus/minus values represent**
 398 **standard deviation ($n=2$).**

Temperature (°C)	Cleanliness (%)	
	99.0 % clean	99.9 % clean
40	99.4 ±0.36	99.7 ±0.12
55	99.8 ±0.06	99.9 ±0.05
70	99.4 ±0.70	99.9 ±0.06

399

400 This particular method of quantifying residual foulant is analogous to the optical method
 401 completed in the fluorescence microscopy portion of the study. As another form of a 2-dimensional
 402 analysis, it can only detect how much surface area has foulant on it but not how tall said foulant is.
 403 Further analysis using the AFM data height mapping should be the next step in quantification of nano-
 404 foulants on surface in a 3-dimensional approach.

405 3.2.2 Force mapping

406 Several force maps were taken in an effort to further identify indicators of residual foulant
 407 materials on the stainless steel surface. Interaction between the custom AFM tip and a clean sample
 408 (cleaned using the aforementioned solvent method in section 2.4.2) were analyzed first to create
 409 baseline attraction and repulsion measurements. It was found that the custom AFM tip consistently had
 410 an adhesion force (approximately 1 nN) to the clean stainless steel surface. The adhesion force was
 411 defined as the minimum deflection of the AFM tip's cantilever when removed from contact with the
 412 surface. This phenomenon was investigated further using samples which were first identified to have
 413 residual deposits by analyzing topography. Although preliminary, results showed that there was a

414 similarity in “clean” areas of the partially fouled coupons and the force interaction on a deposit did not
415 show the adhesion force. Fig. 6 shows the 3-d projection of a force map and the extraction of two plots
416 of vertical deflection as the tip is retracted. Here we can see when the AFM tip retracts from what is
417 seemingly a clean area of the coupon (point A), an approximately 2 nN adhesion force is observed.
418 When the identical map is extracted on the foulant region (point B) there is seemingly no adhesion force
419 observed. This attribute is seemingly quite consistent across various points within the AFM force maps.
420 Validating changes in interaction forces (adhesion forces or otherwise) will help to identify residual
421 deposits when surface topography fails. Future investigation in the area of detection and quantification
422 of nano-foulants should focus in this area.

423 5. Conclusions

424 The current investigation used advanced analytical techniques commonly used in nano materials
425 science and applied them to hygienic design in food process engineering. Specifically, fluorescence
426 microscopy was used to determine the effect of temperature on a dairy type model foulant on stainless
427 steel during exposure to cleaning solution for various times. A Gompertz asymptote model was
428 parameterized and fit to the fluorescence data to generate predictive cleaning equations for visual
429 cleanliness. The predictive equations were used to create samples for analysis using atomic force
430 microscopy (AFM). The AFM was able to characterize residual nano-foulants on the order of $5 \mu\text{m}^2$ as
431 well as identify the lack of fit of the nano-deposit removal when compared to the visually clean model.
432 Interaction forces between a custom AFM tip and stainless steel with and without deposit was
433 investigated. Strong adhesion forces seem to predominate when the tip interacted with clean areas and
434 where areas with residual foulant showed none. The work completed here shows significant advances in
435 the detection and quantification of residual material on food contact surfaces. Advances in this area are
436 necessary for advancing validation procedures for clean in place operations on a commercial scale. The

437 results show the “next level” of detection and quantification of residual foulant material on food contact
438 surfaces, setting a stage for advanced analytical methods for certifying cleanliness of food contact
439 surfaces.

440 Acknowledgements

441 The authors would like to thank the Society of the Chemical Industry for their Seligman APV Fellowship
442 which allowed for the collaborative research completed in this study.

443 References

444 Akhtar, N., Bowen, J., Asteriadou, K., Robbins, P.T., Zhang, Z., Fryer, P.J., 2010. Matching the nano- to the
445 meso-scale: Measuring deposit-surface interactions with atomic force microscopy and
446 micromanipulation. *Food Bioprod. Process.* 88, 341–348. doi:10.1016/j.fbp.2010.08.006

447 Bakeev, K.A., 2010. *Process analytical technology: spectroscopic tools and implementation strategies for*
448 *the chemical and pharmaceutical industries.* John Wiley & Sons.

449 Belda-Galbis, C.M., Pina-Perez, M.C., Espinosa, J., Marco-Celdran, A., Martinez, A., Rodrigo, D., 2014. Use
450 of the modified Gompertz equation to assess the *Stevia rebaudiana* Bertoni antilisterial kinetics.
451 *Food Microbiol.* 38, 56–61. doi:10.1016/j.fm.2013.08.009

452 Bobe, U., Hoffman, J., Sommer, K., Beck, U., Reiners, G., 2007. Adhesion - where cleaning starts 18, S36-
453 39. doi:10.1016/j.tifs.2006.10.019

454 Changani, S.D., Belmar-Beiny, M.T., Fryer, P.J., 1997. Engineering and chemical factors associated with
455 fouling and cleaning in milk processing. *Exp. Therm. Fluid Sci.* 14, 392–406. doi:10.1016/S0894-
456 1777(96)00141-0

457 Chatterjee, T., Chatterjee, B.K., Majumdar, D., Chakrabarti, P., 2014. Antibacterial effect of silver

- 458 nanoparticles and the modeling of bacterial growth kinetics using a modified Gompertz model.
459 *Biochim. Biophys. Acta* 1850, 299–306. doi:10.1016/j.bbagen.2014.10.022
- 460 Chen, M.-Y., Chen, M.-J., Lee, P.-F., Cheng, L.-H., Huang, L.-J., Lai, C.-H., Huang, K.-H., 2010. Towards real-
461 time observation of conditioning film and early biofilm formation under laminar flow conditions
462 using a quartz crystal microbalance. *Biochem. Eng. J.* 53, 121–130. doi:10.1016/j.bej.2010.10.003
- 463 Cole, P.A., Asteriadou, K., Robbins, P.T., Owen, E.G., Montague, G.A., Fryer, P.J., 2010. Comparison of
464 cleaning of toothpaste from surfaces and pilot scale pipework. *Food Bioprod. Process.* 88, 392–
465 400. doi:10.1016/j.fbp.2010.08.008
- 466 Fan, M., Phinney, D.M., Heldman, D.R., 2015. Effectiveness of rinse water during in-place cleaning of
467 stainless steel pipe lines. *J. Food Sci.* 80, E1490–E1497. doi:10.1111/1750-3841.12914
- 468 Fang, H.H., Chan, K.Y., Xu, L.C., 2000. Quantification of bacterial adhesion forces using atomic force
469 microscopy (AFM). *J. Microbiol. Methods* 40, 89–97. doi:10.1016/S0167-7012(99)00137-2
- 470 Favrat, O., Gavaille, J., Aleya, L., Monteil, G., 2012. Real Time Study of Detergent Concentration
471 Influence on Solid Fatty Acid Film Removal Processes. *J. Surfactants Deterg.* 1–7.
472 doi:10.1007/s11743-012-1383-7
- 473 Fickak, A., Al-Raisi, A., Chen, X.D., 2011. Effect of whey protein concentration on the fouling and cleaning
474 of a heat transfer surface. *J. Food Eng.* 104, 323–331. doi:10.1016/j.jfoodeng.2010.11.004
- 475 Forsyth, R.J., Hartman, J.L., Nostrand, V. Van, 2006. Risk management assessment of visible residue
476 limits in cleaning validation. *Pharm. Technol.* 30, 104–114.
- 477 Fryer, P.J., Christian, G.K., Liu, W., 2006. How hygiene happens: Physics and chemistry of cleaning. *Int. J.*
478 *Dairy Technol.* 59, 76–84. doi:10.1111/j.1471-0307.2006.00249.x

- 479 Gillham, C.R., Fryer, P.J., Hasting, A.P.M., Wilson, D.I., 1999. Cleaning-in-Place of whey protein fouling
480 deposits. *Food Bioprod. Process.* 77, 127–136. doi:10.1205/096030899532420
- 481 Gompertz, B., 1825. On the nature of the function expressive of the law of human mortality, and on a
482 new mode of determining the value of life contingencies. *Philos. Trans. R. Soc. London* 115, 513–
483 583.
- 484 Handojo, A., Zhai, Y., Frankel, G., Pascall, M.A., 2009. Measurement of adhesion strengths between
485 various milk products on glass surfaces using contact angle measurement and atomic force
486 microscopy. *J. Food Eng.* 92, 305–311. doi:10.1016/j.jfoodeng.2008.11.018
- 487 Heldman, D.R., Lund, D.B., 2007. *Handbook of Food Engineering*, 2nd ed. CRC Press, Taylor & Francis
488 Group. Boca Raton, FL.
- 489 Hossain, F., Follett, P., Dang Vu, K., Harich, M., Salmieri, S., Lacroix, M., 2016. Evidence for synergistic
490 activity of plant-derived essential oils against fungal pathogens of food. *Food Microbiol.* 53, 24–30.
491 doi:10.1016/j.fm.2015.08.006
- 492 Jeurink, T.J.M., Brinkman, D.W., 1994. The cleaning of heat exchangers and evaporators after
493 processing milk or whey. *Int. Dairy J.* 4, 347–368. doi:10.1016/0958-6946(94)90031-0
- 494 Jones, I., Cullen, P.J., Greene, A., 2012. Using PAT to support the transition from cleaning process
495 validation to continued cleaning process verification. *J. Valid. Technol.* 18.1, 50–56.
- 496 Klahre, J., Flemming, H.C., 2000. Monitoring of biofouling in papermill process waters. *Water Res.* 34,
497 3657–3665.
- 498 Liu, W., Fryer, P.J., Zhang, Z., Zhao, Q., Liu, Y., 2006. Identification of cohesive and adhesive effects in the
499 cleaning of food fouling deposits. *Innov. Food Sci. Emerg. Technol.* 7, 263–269.

- 500 doi:10.1016/j.ifset.2006.02.006
- 501 Mercadé-Prieto, R., Chen, X.D., 2006. Dissolution of whey protein concentrate gels in alkali. *AIChE J.* 52,
502 792–803. doi:10.1002/aic.10639
- 503 Mercadé-Prieto, R., Paterson, W.R., Chen, X.D., Wilson, D.I., 2008. Diffusion of NaOH into a protein gel.
504 *Chem. Eng. Sci.* 63, 2763–2772. doi:10.1016/j.ces.2008.02.029
- 505 Midelet, G., Carpentier, B., 2004. Impact of cleaning and disinfection agents on biofilm structure and on
506 microbial transfer to a solid model food * 262–270. doi:10.1111/j.1365-2672.2004.02296.x
- 507 Moro, A., Gatti, C., Delorenzi, N., 2001. Hydrophobicity of whey protein concentrates measured by
508 fluorescence quenching and its relation with surface functional properties. *J. Agric. Food Chem.* 49,
509 4784–4789. doi:10.1021/jf001132e
- 510 Okorn-schmidt, H.F., Holsteyns, F., Lippert, A., Mui, D., Kawaguchi, M., Lechner, C., Frommhold, P.E.,
511 Nowak, T., Reuter, F., Piqu, B., Cair, C., Mettin, R., 2014. Particle Cleaning Technologies to Meet
512 Advanced Semiconductor Device Process Requirements 3, 3069–3080. doi:10.1149/2.011401jss
- 513 Palabiyik, I., Olunloyo, B., Fryer, P.J., Robbins, P.T., 2014. Flow regimes in the emptying of pipes filled
514 with a Herschel-Bulkley fluid. *Chem. Eng. Res. Des.* 92, 2201–2212.
515 doi:10.1016/j.cherd.2014.01.001
- 516 Schneider, C. a, Rasband, W.S., Eliceiri, K.W., 2012. NIH Image to ImageJ: 25 years of image analysis. *Nat.*
517 *Methods* 9, 671–675. doi:10.1038/nmeth.2089
- 518 Simeone, A., Watson, N., Sterritt, I., Woolley, E., 2016. A Multi-sensor Approach for Fouling Level
519 Assessment in Clean-in-place Processes. *Procedia CIRP* 55, 134–139.
520 doi:10.1016/j.procir.2016.07.023

521 Sinnott, R.K., 1999. Coulson & Richardson's Chemical Engineering, Volume 6: Chemical Engineering
522 Design (4th ed.). Elsevier Butterworth Heinemann.

523 Tiwari, S., Behera, C.R., Srinivasan, B., 2016. Simulation and experimental studies to enhance water
524 reuse and reclamation in India's largest dairy industry. J. Environ. Chem. Eng. 4, 605–616.
525 doi:10.1016/j.jece.2015.12.001

526 Van Asselt, A.J., Van Houwelingen, G., Te Giffel, M.C., 2002. Monitoring System for Improving Cleaning
527 Efficiency of Cleaning-in-Place Processes in Dairy Environments. Food Bioprod. Process. 80, 276–
528 280. doi:10.1205/096030802321154772

529

Figure 1: Color distributions of clean (A) and dirty (B) coupons imaged under fluorescent microscopy. Error bars show standard deviation of samples (n=6).

Figure 2: Comparison of the original images acquired on the fluorescent microscope (top row) the same image after conversion to the clean/dirty image (bottom row). Red pixels in the image represent pixels with a color score higher than 45 and are therefore considered dirty.

Figure 3: Results from the fluorescent microscopy cleaning investigation with sigmoidal model fits (lines) overlaid on the raw data (squares). Each square represents the average of 3 randomized experiments with standard deviations presented as error bars. Dashed lines represent the 95 % confidence interval around each prediction model.

Figure 4: Results from the surface topography investigation using atomic force microscopy.

Figure 5: Figure 5: From left to right is; (1) the original AFM image from JPKSPM analysis, (2) the image converted to black and white, (3) the image converted in to a binary image and (4) the Matlab™ 'strel/disk' identification in the binary image.

Figure 6: 3-dimnesional projection of a height tract on 100 x 100 μm area (top) which was analyzed using AFM force mapping. The vertical deflection of the AFM cantilever during retraction at two points (bottom) are separately plotted.

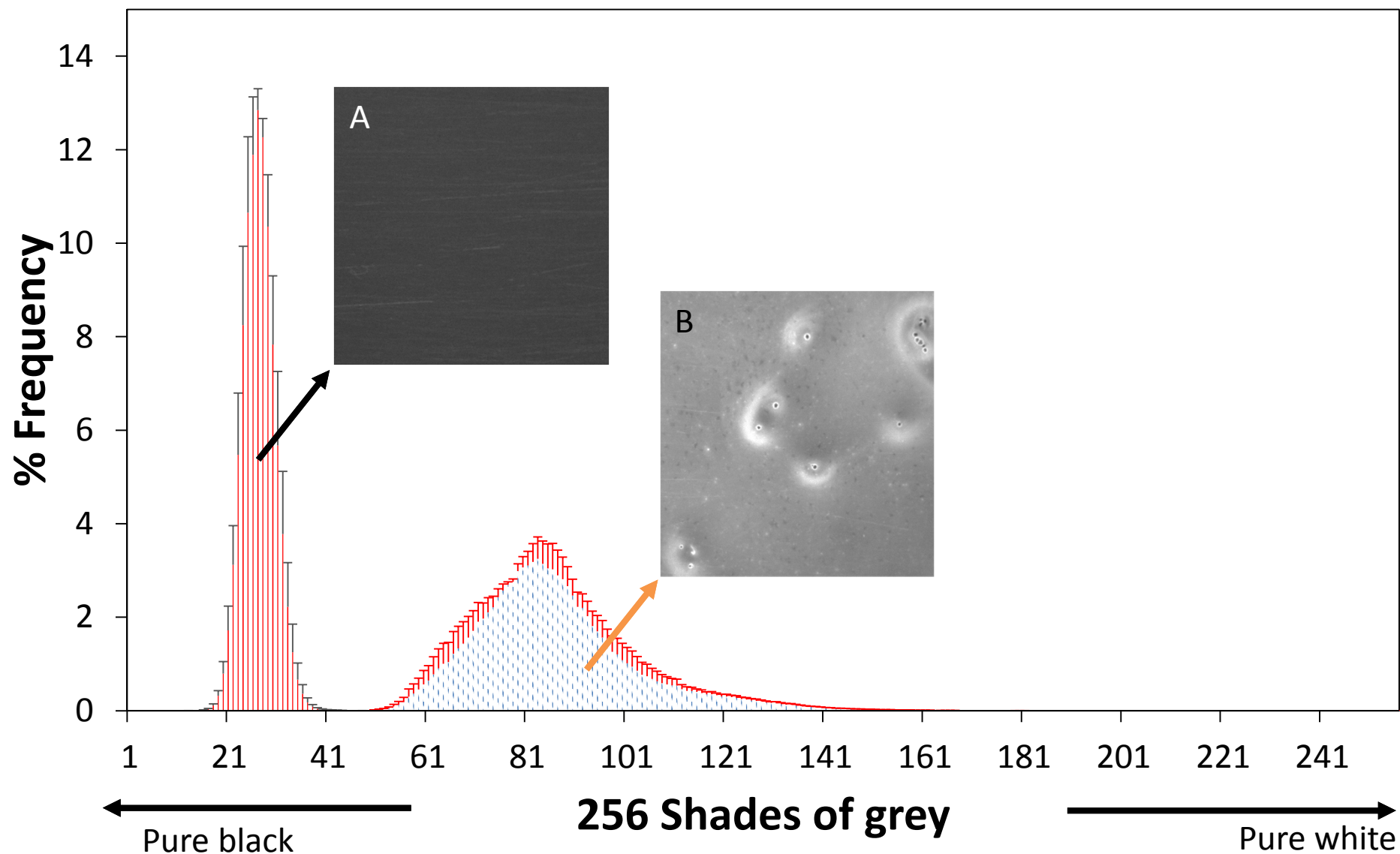


Figure 1: Color distributions of clean (A) and dirty (B) coupons imaged under fluorescent microscopy. Error bars show standard deviation of samples (n=6).

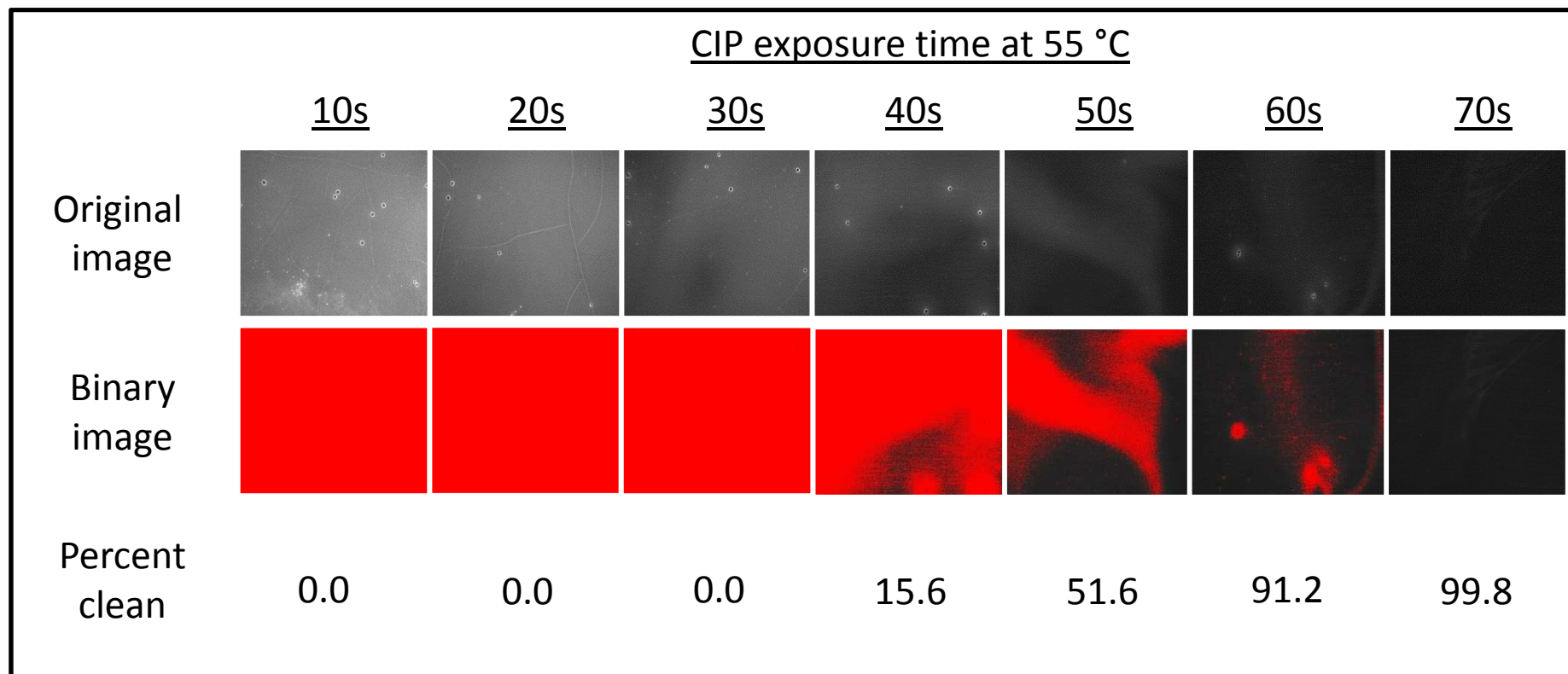


Figure 2: Comparison of the original images acquired on the fluorescent microscope (top row) the same image after conversion to the clean/dirty image (bottom row). Red pixels in the image represent pixels with a color score higher than 45 and are therefore considered dirty.

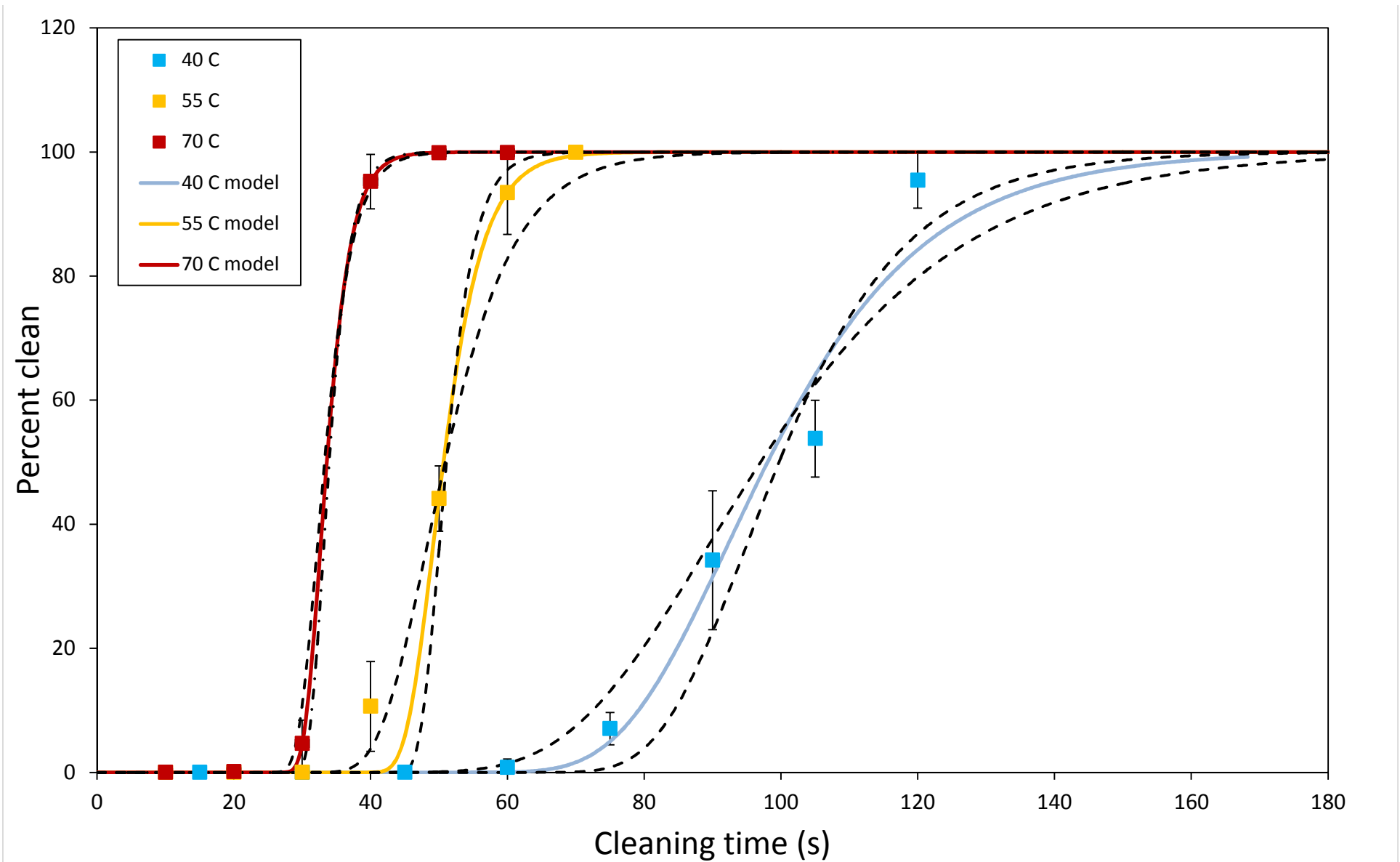


Figure 3: Results from the fluorescent microscopy cleaning investigation with sigmoidal model fits (lines) overlaid on the raw data (squares). Each square represents the average of 3 randomized experiments with standard deviations presented as error bars. Dashed lines represent the 95 % confidence interval around each prediction model.

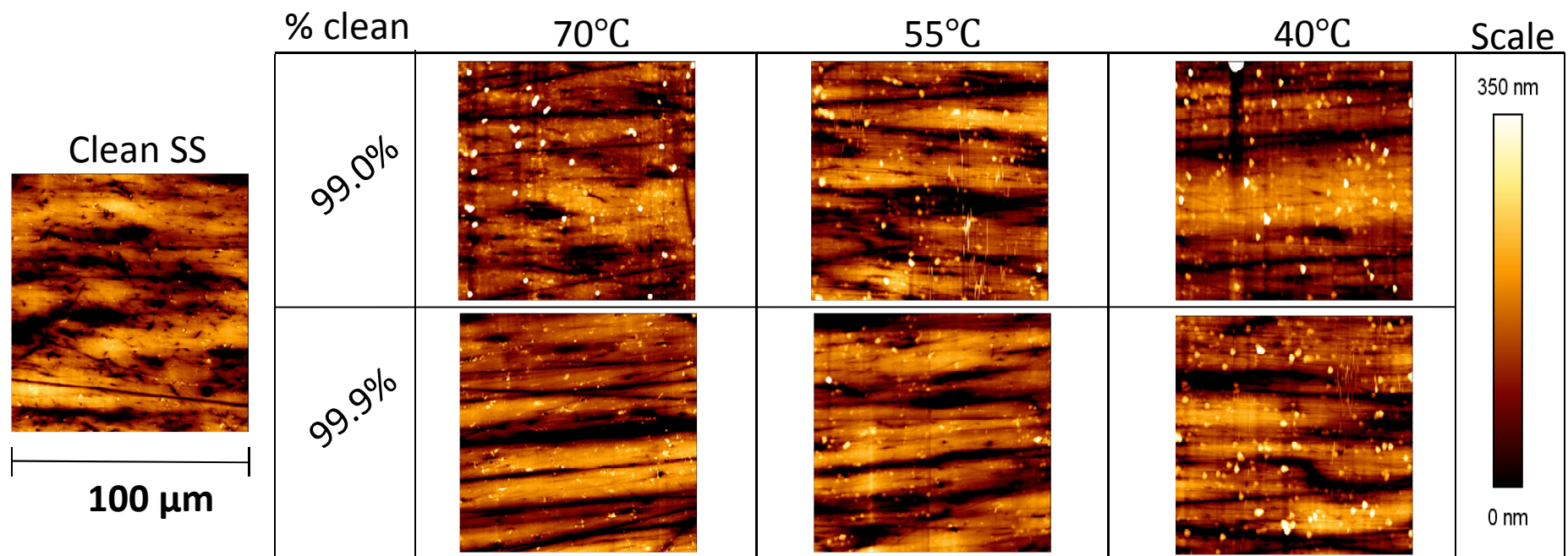


Figure 4: Results from the surface topography investigation using atomic force microscopy.

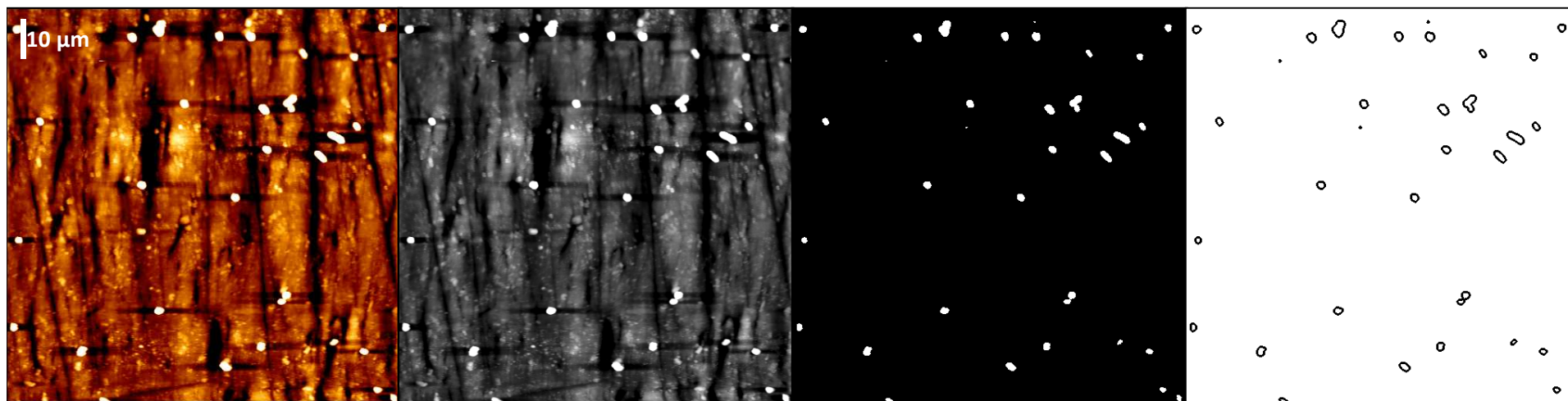


Figure 5: From left to right is; (1) the original AFM image from JPKSPM analysis, (2) the image converted to black and white, (3) the image converted in to a binary image and (4) the Matlab[™] 'strel/disk' identification in the binary image.

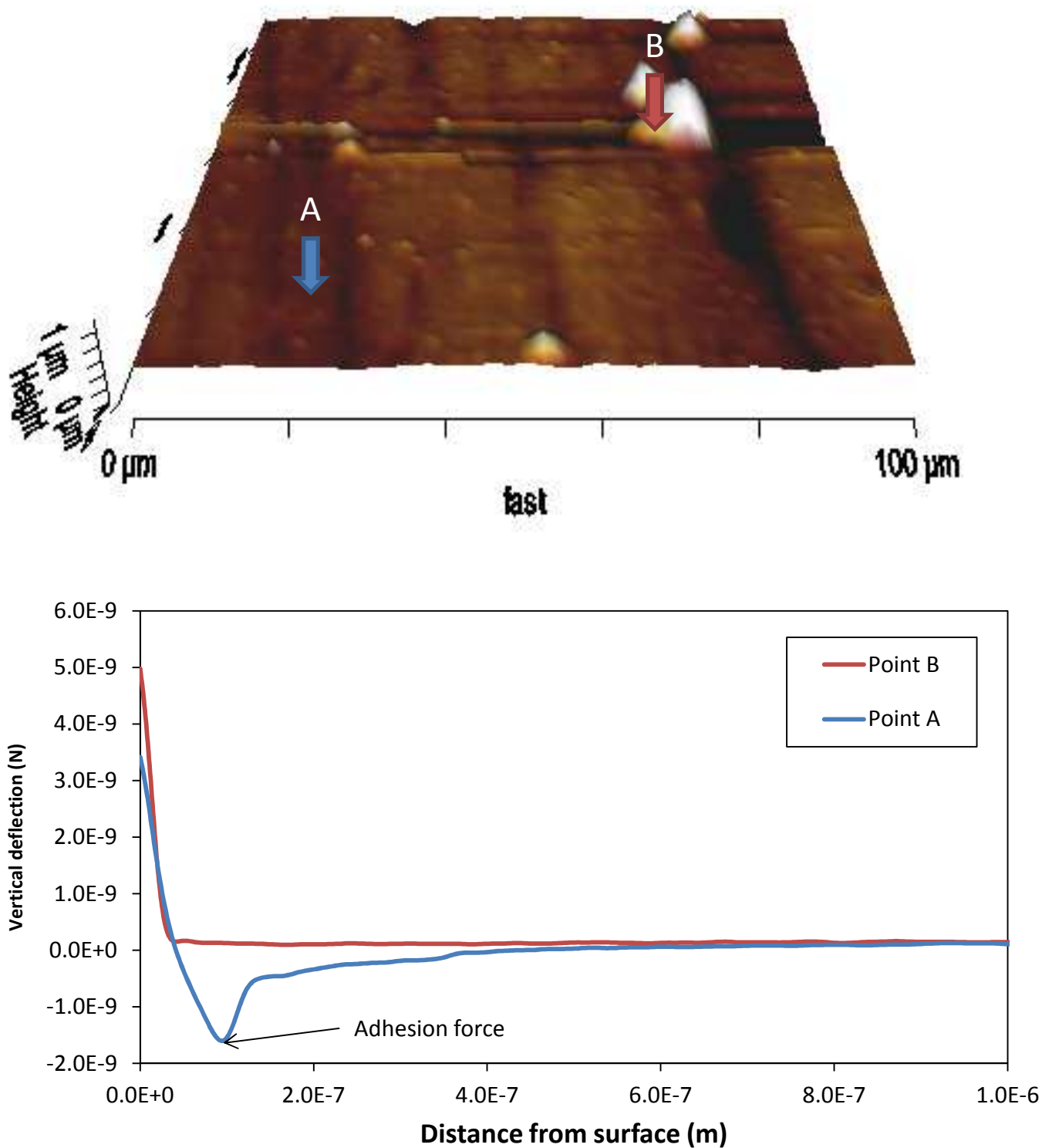


Figure 6: 3-dimensional projection of a height tract on $100 \times 100 \mu\text{m}$ area (top) which was analyzed using AFM force mapping. The vertical deflection of the AFM cantilever during retraction at two points (bottom) are separately plotted.

Highlights

- Fluorescence microscopy quantified visual surface cleanliness
- Visual cleanliness fit a sigmoidal cleaning model for whey protein deposits
- Atomic force microscopy was able to identify invisible deposits
- Invisible deposits as small as $5 \mu\text{m}^2$ could be identified